Supporting Material

A Role for Septins in the Interaction between the *Listeria monocytogenes* Invasion Protein InlB and the Met Receptor

Serge Mostowy, Sébastien Janel, Claire Forestier, Charles Roduit, Sandor Kasas, Javier Pizarro-Cerdá, Pascale Cossart, and Frank Lafont

This file includes:

SUPPLEMENTAL MATERIAL AND METHODS

Atomic force microscopy (AFM)

i. Live cell imaging

AFM was operated in contact mode using Olympus Bio-Lever with a spring constant of 0.006N/m. We applied a constant force of 100pN while scanning at 0.3Hz. Images were corrected (plane fit) using Veeco's Nanoscope 7.30 software. One image, representative of 5, is shown for each condition.

ii. Surface Met quantification experiments

Tip coating was performed using established protocol known to keep proteins functionality intact and applied on living cells as we previously published (1, 2). InlB was used at a concentration of 50µg/ml. We used Veeco DNP cantilevers with a nominal spring constant of 0.06N/m and a nominal tip radius of 20nm. Experiments were done in force-volume mode operating in MEM without Phenol Red - (10mM) Hepes buffer (pH 7.4) at a scan frequency of 2Hz on 20µm^2 areas (64x64), with a relative trigger of 50nm on the cantilever deflection (i.e. 3nN nominal). We scanned 6 cells each with a different tip (24576 force curves). Events occurring immediately after tip-sample contact were considered as nonspecific tip-surface adhesion events and were systematically discarded from our analysis. Force-distance curves were analysed as we previously described (2) and binding-unbinding events on the retraction curve were detected according to their shape and size characteristics by a fuzzy logic algorithm fully described in (3). Briefly, we considered unbinding events based on the vertical segment and the angle with the baseline in order to take into account both V-shaped (Δ) and plateau-like events (*) (Fig. 2 *C*). *p*-values (Fig. 3 *C*) were calculated using the the Mann-Whitney test in R (2.10).

iii. Unbinding force and tether experiments

Cantilever spring constant was determined using Veeco's thermal tune calibration tool. We operated the AFM in the force-volume mode on 2µm^2 areas (32x32 points) on different positions at the cell surface, using a relative trigger of 50nm on the cantilever deflection. Measurements were performed under similar conditions on different days with different cells and functionalized tips. We used 25600 curves obtained from 12 cells and 7 tips to perform a statistical analysis of our results. Loading rate and pulling velocity experiments were conducted with Veeco's MLCT cantilevers with nominal spring constant 0.01N/m. The fuzzy logic algorithm was adapted to detect the V-shaped unbinding events and the force plateaus due to membrane tether elongation (4). To discriminate tethers, we applied a distance threshold of 400nm. For force measurements and loading rate experiments shown in Figure 3, only V-shaped unbinding events were considered. Rupture forces, F_R, were determined as described (5, 6). Gaussian curves were used to fit histogram distributions. Force spectroscopy with decoy-Met purified protein was performed after the decoy-Met has been deposited on a glass surface through a nitrilotriacetic acid (NTA) that ensure covalent and oriented binding with the protein (7). Statistical analysis was performed using R (2.10). Where provided are the peak position mean values ± s.e.m (unbinding force experiments, Fig. 3) and mean ± s.d (tether experiments, Fig. 4). The statistical difference between SEPT2- and SEPT11-depleted cell viscosities was determined using a Prism software internal test (Fig. 4 *B*). A Student's *t*-test was used to statistically compare the percentage of tether events for siRNA treatements (Fig. 4 *D*).

iv. Elasticity experiments

Local elastic (or Young's) modulii were obtained based on the Hertzian model for elastic indentations as previously described (2). Young's modulii were calculated at 50nm indentation depths and mapped onto the topograms (1, 2). 3D elasticity images (i.e. Fig. 5 *A*) were calculated from 50μm^2 force-volume data (128x128 points) and drawn using Blender software.

SUPPLEMENTAL TEXT

Dynamic force spectroscopy experiment in terms of the Bell-Evans model

The dissociation rate constant at a given force $k_d(f)$ is defined as:

$$k_d(f) = k_d^0 \exp\left(\frac{f\Delta x}{k_B T}\right)$$

where k_d^0 is the intrinsic dissociation rate (zero force), Δx the width of the energy barrier, f the constant applied force, k_B the Boltzmann constant and T the temperature. The dissociation constant (K_D) is related to the association rate constant (k_a^0) and to the dissociation rate constant (k_d^0) as:

$$K_D = \frac{k_d^0}{k_a^0}$$

with K_D expressed in M, k_d^0 in s^{-1}, and k_a^0 in mol^{-1} s^{-1}. If the force increases at a constant rate r_f, then the most probable unbinding force f^* can be written as:

$$f^* = \frac{k_B T}{\Delta x} \ln \frac{\Delta x}{k_d^0 k_B T} + \frac{k_B T}{\Delta x} \ln(r_f)$$

The unbinding herein means overcoming one or more energy barrier.

Tether pulling force

The mechanics of membrane tether extraction depends on the effective viscosity and the threshold extraction force as determined in micropipette experiments (8-10) and laser tweezers (11). For pulling rates < 40μm s^{-1}, the pulling force (F) is characterized by an effective viscosity (η_{eff}) and the tether growth velocity (V_t) according to a well characterized relationship (12):

$$F = F_0 + 2\pi\eta_{eff} V_t$$

Of note, with the exception of neuronal growth cones, the tether force at zero velocity depends on tether length but the radius, at a fixed apparent surface tension, is independent of tether length (12). The threshold force F_0 can be extrapolated from the linear equation governing the force extraction and pulling velocity relationship (9). It is thus different than the global interaction forces analysed (Fig. 3 *B*), and importantly refers only to those unbinding events occurring at 'long distances' (Fig. 4 *A* and events labeled with a * on Fig. 2 *C*).

Septin discussion

Our data show different roles for septins during InlB-Met interactions, and highlight different functions for SEPT2 and SEPT11. SEPT2 and SEPT11 belong to different septin groups (the SEPT2 and SEPT6 groups respectively) (13) and have been associated to different septin complexes, in particular the crystallized SEPT2-SEPT6-SEPT7 complex (14) and the SEPT7-SEPT9-SEPT11 (15) or SEPT5-SEPT7-SEPT11 (16) complexes. Whether or not the different functions of SEPT2 and SEPT11 are

achieved in the framework of any of these reported complexes, or even as individual septins, is currently unknown. It has been proposed that members of the SEPT6 group are interchangeable, at least in the context of the SEPT2-SEPT6-SEPT7 complex (17, 18). Thus, some of the control-like phenotypes observed in cells depleted for SEPT11 may be because SEPT6 group members are partially redundant. Nevertheless, cells depleted for SEPT11 do not present all the control cell phenotypes (i.e. cell morphology, increased Met expression, effective viscosity, cell elasitcity), suggesting that other SEPT6 group members cannot fully substitute for SEPT11.

The situation is different for SEPT2. From the recent structural data, septins are ordered in the isolated complex as SEPT7-SEPT6-SEPT2-SEPT2-SEPT6-SEPT7 (14). As the central subunit in this septin complex, SEPT2 has so far not been described as 'replaceable' by other septins. All our findings (i.e. cell morphology, decreased Met expression, effective viscosity, cell elasitcity), motivated by the original observation that SEPT2-depletion has a negative impact on bacterial invasion (19), consistently demonstrate that SEPT2 is not replaceable.

As we show in this manuscript, there are several reasons why SEPT2-depleted cells are less permissive to *Listeria* entry, and SEPT11-depleted cells are more permissive to *Listeria* entry. SEPT2-depleted cells are less permissive to *Listeria* InlB-mediated entry because cells are smaller (Fig. 1), less Met is available at the cell surface (Fig. 2), and Met receptor is not functionally anchored to the actin cytoskeleton (Figs. 3 and 4). On the other hand, SEPT11-depleted cells are more permissive to *Listeria* entry because cells are bigger (Fig. 1), more Met is available at the cell surface (Fig. 2), and a population of Met receptors remain functionally anchored to the actin cytoskeleton (Figs. 3 and 4).

We have previously shown that septin collars are recruited to the site of bacterial entry, and that SEPT2 depletion eliminates the recruitment of these collars (19). SEPT11 is not essential for the recruitment of septin collars (20, 21) (unpublished observations). Thus, differences in septin collar recruitment to the site of bacterial entry upon SEPT2- versus SEPT11-depletion is likely another contributing factor to differences in *Listeria* entry. However, we do not yet fully understand the role of septin collar recruitment to the site of bacterial entry (22, 23), and in this manuscript we focus on the role of septin in the functional interaction between InlB and Met receptor.

REFERENCES

1. Yersin, A., H. Hirling, S. Kasas, C. Roduit, K. Kulangara, G. Dietler, F. Lafont, S. Catsicas, and P. Steiner. 2007. Elastic properties of the cell surface and trafficking of single AMPA receptors in living hippocampal neurons. Biophys. J. 92:4482-4489.
2. Roduit, C., F. G. van der Goot, P. De Los Rios, A. Yersin, P. Steiner, G. Dietler, S. Catsicas, F. Lafont, and S. Kasas. 2008. Elastic membrane heterogeneity of living cells revealed by stiff nanoscale membrane domains. Biophys. J. 94:1521-1532.
3. Kasas, S., B. M. Riederer, S. Catscicas, B. Capella, and G. Dietler. 2000. Setup for observing living cells using a commercial atomic force microscope. Rev. Sci. Instrum. 71:4338-4341.
4. Muller, D. J., J. Helenius, D. Alsteens, and Y. F. Dufrene. 2009. Force probing surfaces of living cells to molecular resolution. Nat. Chem. Biol. 5:383-390.

5. Afrin, R., and A. Ikai. 2006. Force profiles of protein pulling with or without cytoskeletal links studied by AFM. Biochem. Biophys. Res. Comm. 348:238-244.
6. Afrin, R., T. Yamada, and A. Ikai. 2004. Analysis of force curves obtained on the live cell membrane using chemically modified AFM probes. Ultramicroscopy 100:187-195.
7. Chevalier, S. b., C. Cuestas-Ayllon, V. Grazu, M. Luna, H. Feracci, and J. M. de la Fuente. 2010. Creating biomimetic surfaces through covalent and oriented binding of proteins. Langmuir 26:14707-14715.
8. Shao, J. Y., and F. M. Hochmuth. 1996. Micropipette suction for measuring piconewton forces of adhesion and tether formation from neutrophil membranes. Biophys. J. 71:2892-2901.
9. Girdhar, G., and J. Y. Shao. 2004. Membrane tether extraction from human umbilical vein endothelial cells and its implication in leukocyte rolling. Biophys. J. 87:3561-3568.
10. Girdhar, G., and J. Y. Shao. 2007. Simultaneous tether extraction from endothelial cells and leukocytes: observation, mechanics, and significance. Biophys. J. 93:4041-4052.
11. Dai, J., and M. P. Sheetz. 1995. Mechanical properties of neuronal growth cone membranes studied by tether formation with laser optical tweezers. Biophys. J. 68:988-996.
12. Hochmuth, F. M., J. Y. Shao, J. Dai, and M. P. Sheetz. 1996. Deformation and flow of membrane into tethers extracted from neuronal growth cones. Biophys. J. 70:358-369.
13. Weirich, C. S., J. P. Erzberger, and Y. Barral. 2008. The septin family of GTPases: architecture and dynamics. Nat. Rev. Mol. Cell Biol. 9:478-489.
14. Sirajuddin, M., M. Farkasovsky, F. Hauer, D. Kuhlmann, I. G. Macara, M. Weyand, H. Stark, and A. Wittinghofer. 2007. Structural insight into filament formation by mammalian septins. Nature 449:311-315.
15. Nagata, K.-i., T. Asano, Y. Nozawa, and M. Inagaki. 2004. Biochemical and cell biological analyses of a mammalian septin complex, Sept7/9b/11. J. Biol. Chem. 279:55895-55904.
16. Xie, Y., J. P. Vessey, A. Konecna, R. Dahm, P. Macchi, and M. A. Kiebler. 2007. The GTP-binding protein Septin 7 is critical for dendrite branching and dendritic-spine morphology. Curr. Biol. 17:1746-1751.
17. Kinoshita, M. 2003. Assembly of mammalian septins. J. Biochem. (Tokyo) 134:491-496.
18. Ono, R., M. Ihara, H. Nakajima, K. Ozaki, Y. Kataoka-Fujiwara, T. Taki, K.-i. Nagata, M. Inagaki, N. Yoshida, T. Kitamura, Y. Hayashi, M. Kinoshita, and T. Nosaka. 2005. Disruption of Sept6, a fusion partner gene of MLL, does not affect ontogeny, leukemogenesis induced by MLL-SEPT6, or phenotype induced by the loss of Sept4. Mol. Cell. Biol. 25:10965-10978.
19. Mostowy, S., T. Nam Tham, A. Danckaert, S. Guadagnini, S. Boisson-Dupuis, J. Pizarro-Cerda, and P. Cossart. 2009. Septins regulate bacterial entry into host cells. PLoS ONE 4:e4196.
20. Mostowy, S., A. Danckaert, T. N. Tham, C. Machu, S. Guadagnini, J. Pizarro-Cerda, and P. Cossart. 2009. Septin 11 restricts InlB-mediated invasion by *Listeria*. J. Biol. Chem. 284:11613-11621.
21. Mostowy, S., M. Bonazzi, M. Hamon, T. N. Tham, A. Mallet, M. Lelek, E. Gouin, C. Demangel, R. Brosch, C. Zimmer, A. Sartori, M. Kinoshita, M.

Lecuit, and P. Cossart. 2010. Entrapment of intracytosolic bacteria by septin cage-like structures. Cell Host Microbe 18:433-444.
22. Mostowy, S., and P. Cossart. 2009. Cytoskeleton rearrangements during *Listeria* infection: Clathrin and septins as new players in the game. Cell Motil. Cytoskel. 66:816-823.
23. Mostowy, S., and P. Cossart. 2009. From pathogenesis to cell biology and back. Cell Host Microbe 5:510-513.

SUPPLEMENTAL FIGURE LEGENDS

SUPPLEMENTAL FIGURE S1 Met mapping on the surface of living cells. Met mapping was performed for control (CTRL), SEPT2-depleted, SEPT11-depleted, or latrunculin B (LatB)-treated cells. Each image represents an AFM scan of $2\mu m^2$ made of 32x32 pixels (force curves). Height is represented as false color ranging from dark (low) to light (high). Blue * indicates positions where unbinding events were detected.

SUPPLEMENTAL FIGURE S2 InlB-Met interactions on a model surface. *(A)* Surface characterization of decoy-Met oriented and covalently attached to a glass surface by AFM. Top is a height image (color scale 20nm) showing a homogeneous functionalization of the surface by Met. Bottom left shows an image obtained after scratching $1\mu m^2$ of the surface with the AFM tip. The resulting height profile (bottom right) shows the height of the protein layer on the glass to be about 8nm. Scale bar = 500nm. *(B)* Top shows representative examples of retraction force curves recorded at the Met surface with (black) and without (brown) interaction events. Bottom bar plots represent the probability of having 0, 1, 2, or 3 events on a curve. *(C)* Dynamic force spectroscopy of the decoy-Met-InlB interaction representing the unbinding force (pN) versus loading rate (nN s^{-1}). Force increases linearly with the loading rate and gives values of Δx and k_d^0 similar to those obtained on living cells. *(D)* Energy diagram of the InlB-Met interaction (single energy barrier).

SUPPLEMENTAL FIGURE S3 HeLa cells were treated with control (CTRL), SEPT2, or SEPT11 siRNA. Whole-cell lysates of siRNA-treated cells were immunoblotted for GAPDH, actin, SEPT2, or SEPT11 to show the efficiency of septin depletion. GAPDH is shown as a loading control.

Mostowy et al. Supp. Figure S1

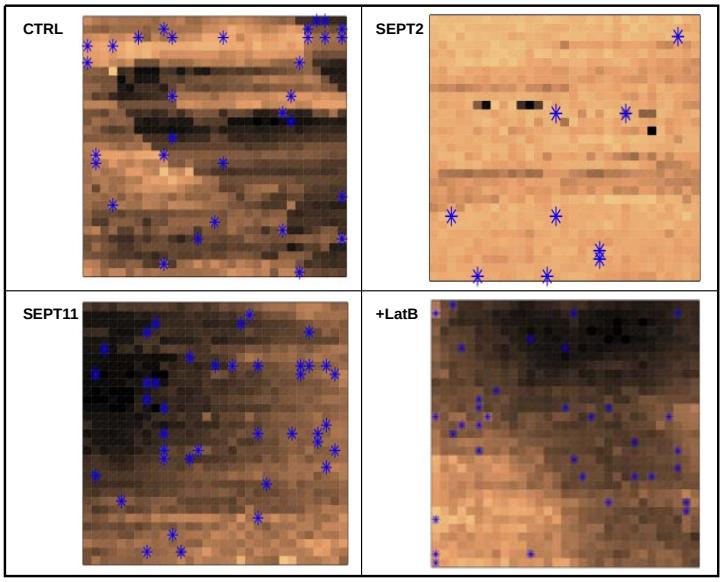

Mostowy et al. Supp. Figure S2

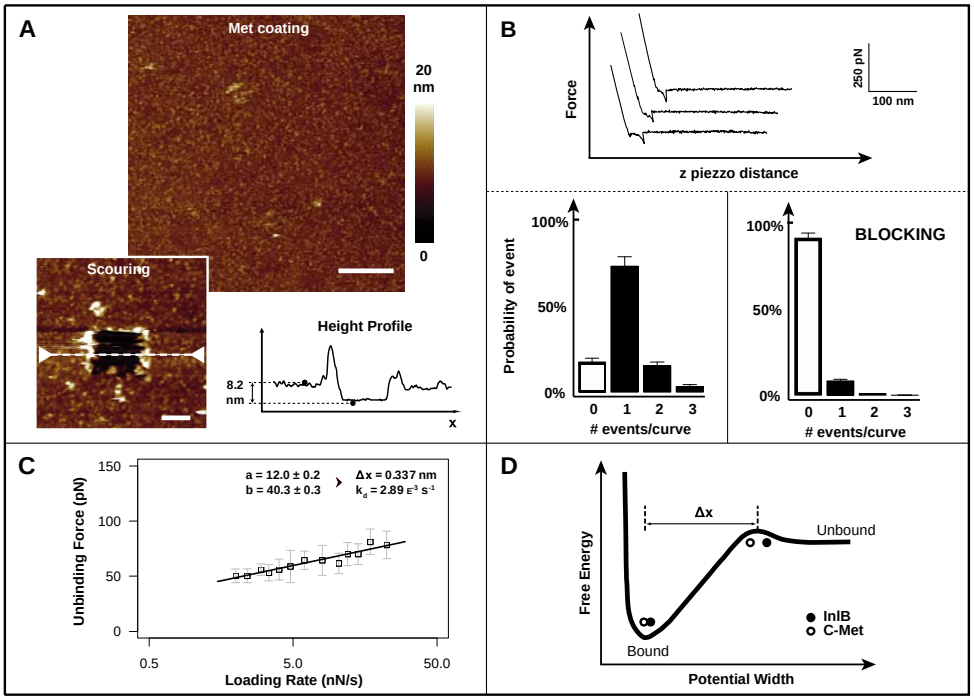

Mostowy et al. Supp. Figure S3